$L_{2,3}VV$ and MVV Auger spectra of copper

H. H. Madden
Sandia Laboratories, 5114, Albuquerque, New Mexico 87185

D. M. Zehner and J. R. Noonan
Solid State Division, Oak Ridge National Laboratory, Oak Ridge, Tennessee 37830

(Received 7 November 1977)

Electron-excited integral $L_{2,3}VV$ and MVV Auger spectra from clean copper surfaces are presented and compared with x-ray excited $L_{2,3}VV$ spectra, with other electron-excited derivative MVV spectra, and with the results of atomic-model and band-theory calculations. Our $L_{2,3}VV$ spectra agree well with the x-ray-excited results in both line shape and L_3VV-to-L_2VV integrated-intensity ratio. Recent atomic-model interpretations of these spectra by McGuire are briefly reviewed and found, especially for the L_3VV spectrum, to provide a very good explanation of the spectra: the multiplet splitting mechanism is responsible for the major peaks, and satellite-intensity contributions resulting from Coster-Kronig L_1L_2V, L_1L_3V, and L_2L_3V transitions give rise to the low-energy portions of the spectra. Our MVV spectra also have sharp features with shapes that are in agreement with atomic-model calculations. The experimental $M_{2,3}VV$-to-M_1VV integrated-intensity ratio is much larger than 3 to 1, and varies with primary-electron-beam energy, indicating that satellite intensity contributions make up part of the MVV signals. The sharp features in these spectra, however, do not change with variations in primary-beam energy from 119 to 3000 eV indicating that they are not dependent upon satellite intensity. The experimental M_3VV-to-M_2VV integrated-intensity ratio also remains unchanged at 1.3 to 1 for the same variation in primary-beam energy. A broad high-energy shoulder forms part of the MVV spectra, especially for the M_1VV signal. This feature of the MVV line shapes is not in agreement with the atomic-model calculations. It is also not simply related to the undistorted valence-band density of states for copper. Comparison of our M_1VV signal with recent band-theory arguments of Cini and of Sawatzky indicates that the MVV line shapes are explainable in terms of distortions in the Auger core-valence-valence signals from narrow-valence-band metals that are expected to occur as a result of hole-hole interactions in the two-hole final-state configuration. Estimates of the hole-hole repulsion energy based on these comparisons are discussed in light of an earlier estimate of this interaction energy based on L_3VV data.

I. INTRODUCTION

Despite its long recognized[1] potential as a valence-band spectroscopy, Auger-electron spectroscopy (AES) has had very limited application in measuring the valence-band density-of-states (DOS) of solids. Although valence-band origins have been ascribed to features of core-valence-valence (CVV) spectra of a number of materials, much of the identification of CVV line shapes as being "bandlike" seems to have been based, partially at least, on the greater breadth of these lines in comparison with core-level photoelectron lines and with other Auger lines for transitions that do not involve the valence electrons. Only recently have detailed comparisons of integral CVV Auger line shapes with theoretical densities of states and/or with line shapes from other valence-band spectroscopies indicated that the CVV line shapes can be simply understood in terms of unperturbed one-electron valence-band DOS for Al,[2,3] Si,[4] Li,[5] Ti,[6] and Ag.[7] These comparisons indicate that the transition-matrix elements play an important role in determining the Auger line shape. Only for silicon, however, has a complete independent-particle calculation—specifically retaining the transition-matrix elements—been made[8] that resulted in improved agreement between the experimental Auger line shape and theory. These recent results provide encouraging indications that AES may indeed be more successfully applied as a valence-band spectroscopy than it has been in the past. The two-hole final state in AES makes it a unique method of investigating the electronic structure of materials. This aspect of AES will be seen to be important in the CVV lines of copper discussed in this paper.

In contrast to the successful valence-band-DOS interpretations for the CVV signals from Al, Si, Li, Ti, and Ag, the integral, high-resolution CVV lines from some other materials (in general, d-band metals) have shapes that have no simple relationship to their valence-band DOS. The $L_{2,3}VV$ copper signals, among the most studied of CVV lines, are of this latter type. All of the prior investigations of the shapes of these lines[9-13] have involved photon excitation in experimental systems designed for high-resolution x-ray photoelectron spectroscopy (XPS). Current interpretations[12-14] of the shapes of these lines completely ignore the

valence-band DOS of copper and treat the spectra as superpositions of atomiclike Auger lines. The Auger decays of the initial vacancy sites in these metals proceed as if they involved isolated atoms. This behavior is ascribed[13, 15-18] to hole-hole interactions (electron-correlation effects) in the narrow $3d$ bands that make up the majority of the valence-electron structure of Cu. Thus, although the shapes of the $L_{2,3}VV$-AES lines do not offer information on the unperturbed valence-band DOS of Cu, investigation of these lines does offer a means of studying electron-correlation effects in this d-band metal.

The MVV lines are the only other CVV lines of copper from which valence-band-DOS information has been sought. Despite the fact that the final-state configuration for the MVV transitions should be the same as for the $L_{2,3}VV$ transitions, the MVV line shapes differ markedly from the $L_{2,3}VV$ line shapes. Interpretation of the MVV line shapes has been somewhat ambiguous with both unperturbed valence-band-DOS information as well as atomic-like features suggested[19] as being represented in the shapes. These earlier MVV data were obtained[19] with electron excitation and were in the derivative mode, uncorrected for electron-loss-related distortions. Some structure in these spectra was explained in terms of plasmon losses.

In this paper, electron-excited copper $L_{2,3}VV$ and MVV spectra are presented in the integral-current $[N(E)]$ mode, i.e., the energy distribution of these integral Auger signals are obtained from the first derivative with respect to energy of the total collected current in our retarding-field analyzer. These data are the first electron-excited $L_{2,3}VV$ spectra presented with sufficient resolution to allow direct comparison with the photon-excited spectra. As one should expect, the mode of excitation is not significant in determining the shapes of these spectra and hence our $L_{2,3}VV$ results support the atomic-model interpretation of the shapes of the $L_{2,3}VV$ curves. Deconvolution techniques[20] were required to achieve resolution in our spectra comparable to that of the high-resolution XPS $L_{2,3}VV$ results. Comparison is made between our $L_{2,3}VV$ results and recently published examples of photon-excited $L_{2,3}VV$ spectra[9-13] enabling an evaluation of our data reduction procedures. Good agreement is found in the relative locations in energy of the peaks in the $L_{2,3}VV$ spectra and there is also reasonable agreement in the L_3VV-to-L_2VV integrated-intensity ratios. In order to facilitate a comparison of our MVV spectra with the $L_{2,3}VV$ results and with the results of theory and of other valence-band spectroscopies, a brief review of the current atomic-model arguments concerning the shapes of the $L_{2,3}VV$ spectra is given.

The MVV copper spectra discussed in this paper are the first to be presented in the $N(E)$ form, with loss-related features removed. Despite the fact that the MVV line shapes differ markedly from that of the L_3VV signal, they still exhibit sharp features that suggest atomic-model interpretations. Thus, our MVV spectra are first compared with the results of purely atomic-model calculations. Experimental $M_{2,3}VV$-to-M_1VV integrated-intensity ratios indicate the presence of appreciable satellite intensity in the MVV signals. This is in agreement with atomic-model calculations, as are the shapes of the sharp features in our MVV lines. The major lack of agreement is in a broad high-energy structure that appears in the experimental MVV curves and not in the atomic-model-calculation results.[21] Lack of variation of the MVV line shapes with changes in primary-electron-beam energy from 150 to 3000 eV indicates that the shapes of neither the sharp nor the broad features are significantly influenced by satellite intensity.

Identification of the broad structure in the MVV signal simply with the self-fold of the unperturbed copper total [19a]DOS is found to be incorrect. An interpretation that is more promising, in terms of the new valence-band information it offers, is found in recent theoretical papers by Cini[16] and by Sawatzky[18] that consider the distortions to be expected in the CVV Auger signals from narrow valence-band metals caused by electron correlation effects (hole-hole repulsions). As stated by Sawatzky,[18] these effects will cause "the Auger spectrum (to consist) of a strong narrow, atomic-like peak with a less intense broad band like spectrum appearing at higher kinetic energies." Since this is a good qualitative description of the line shapes of our MVV spectra, these spectra are analyzed in our paper in terms of the predictions of these new theoretical results.

II. EXPERIMENTAL

The Auger spectra were obtained using a four-grid (low-energy-electron-diffraction optics) retarding-field analyzer (Varian Corp.) that has an energy resolution of 0.4%. The primary electron beam was normally incident to the sample surface. Data were obtained from (100) and (110) copper surfaces. The energy of the primary beam was 3 keV for recording the $L_{2,3}VV$ spectra and 1.5 keV, with a number of exceptions (*vide infra*), for recording the MVV spectra. Primary beam currents were constant during the recording of an Auger spectrum and values varied from 2 μA for the $M_{2,3}VV$ spectra to 40 μA for the $L_{2,3}VV$ spectra. A modulation voltage of 1-V peak to peak was used for all measurements. A PAR Model 121 lock-in amplifier was used to amplify the detected signal

and data averaging was performed using a Nicolet Model 1072 signal averager. During all measurements the sample was near room temperature and the base pressure of the vacuum system was below 10^{-7} Pa. Surface cleaning techniques utilized argon-ion bombardment and annealing at 400°C. Surface contaminants were below the Auger-analyzer detection limits during data acquisition.

The data were taken in the $dN(E)/dE$ mode. The secondary-electron background was removed in the cases of the MVV spectra using a correction technique described by Sickafus.[22] This correction was applied directly to the $dN(E)/dE$ data. The background in the $L_{2,3}VV$ spectra was essentially flat and only a zero-suppression correction (or at most a linear background correction) was applied for these data. After background correction the Auger signal is generally characterized by a "steplike" or "plateau-like" structure on its low-energy side. This low-energy tail is due to inelastic losses suffered by some of the Auger electrons in leaving the solid. This structure is illustrated by curve S in Fig. 1 which gives the M_1VV background-corrected integral Auger signal from a (100) copper surface. This loss-related distortion as well as distortions due to instrumental broadening must be removed by deconvolution techniques. Because of the low-energy steplike structure in curve S,

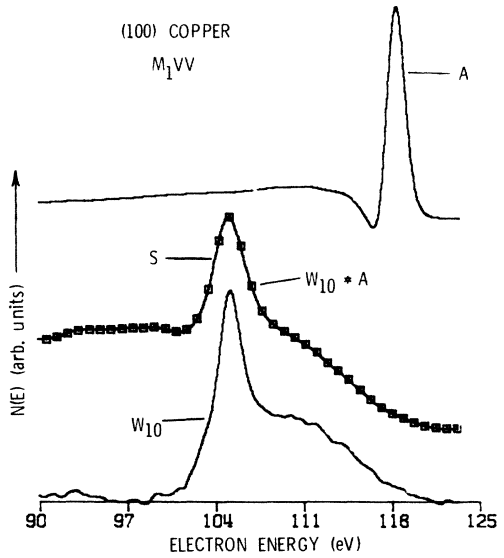

FIG. 1. M_1VV spectrum from a clean (100) copper surface. Curve S—AES signal after correction for secondary-electron background but before deconvolution. Curve A—characteristic loss spectrum used as the system response function in deconvolution; W_{10}—the result of ten (van Cittert) deconvolution iterations using curves S and A; squares plotted on top of curve S give the convolution product of curve W_{10} with A. Zero levels for curves S and A and for the convolution product W_{10} *A are set on the right-hand side of each curve.

Fourier-transform methods of deconvolution are impractical. An iterative (van Cittert) deconvolution technique[20] was used.

The system-response function needed in deconvolution was assumed to be adequately represented by the near-elastic energy spectrum of electrons backscattered from the sample surface when that surface is bombarded with a beam of monoenergetic electrons with energy equal to the threshold energy of the Auger signal. This characteristic-loss spectrum (CLS) gives a measure, in reflection, of the "extrinsic" (or characteristic) energy losses suffered by some of the Auger electrons before they are analyzed and detected, as well as of the instrumental broadening of the spectrometer. Because of the differences in emission geometry between the internal Auger source and the backscattered electrons, some scaling of the elastic peak of the CLS curve with respect to the energy-loss tail is required in order to bring the deconvoluted curve to zero on its low-energy side. Curve A in Fig. 1 depicts the CLS signal used in deconvoluting these M_1VV data. Curve W_{10} in Fig. 1 is the result of ten van Cittert deconvolution iterations using the data function S and the system-response function A. As an indication of the quality of the deconvoluted curve, the convolution product of W_{10} with A is plotted in Fig. 1 as squares on top of the original data function S. The agreement between this convolution product and S indicates that the deconvolution has been performed properly.

III. RESULTS AND DISCUSSION

A. $L_{2,3}VV$ spectra

The total deconvoluted $L_{2,3}VV$ spectra from a (110) surface are plotted in Fig. 2. The L_3VV spectrum from a (100) surface is plotted in Fig. 3. In the latter figure the high-energy end of the L_3VV spectrum has been arbitrarily set equal to zero although our complete $L_{2,3}VV$ spectra (Fig. 2), as well as photon-excited examples of these spectra,[13] indicate that the intensity does not actually go to zero between the L_2VV and L_3VV spectra. Except for this arbitrary zero suppression, the L_3VV signals in Figs. 2 and 3 do not differ significantly in shape, which indicates that the shape of the L_3VV signal is independent of the difference in crystallographic orientation between the (100) and (110) surfaces. This is to be expected since, with the retarding-grid analyzer used in these measurements, this signal is angularly integrated over a large portion of the backward hemisphere.

The peaks in the $L_{2,3}VV$ spectra in Fig. 2 have been labeled A–H to correspond to the L_3VV labeling of Roberts, Weightman, and Johnson[12]

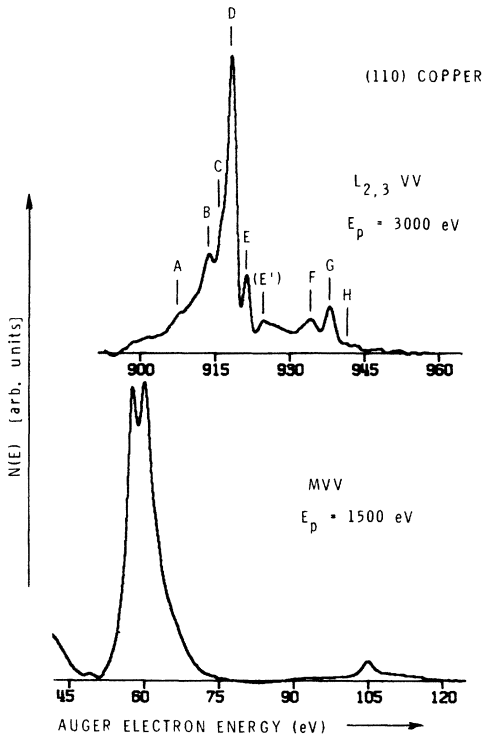

FIG. 2. Deconvoluted $L_{2,3}VV$ (4 iterations) and total MVV (10 iterations) spectra from a clean (110) surface. Peak labels on the $L_{2,3}VV$ spectra correspond to atomic-model peak locations (Ref. 14).

and the extension of that labeling by McGuire[14] to the L_2 VV features. Comparison of our electron-excited deconvoluted $L_{2,3}VV$ spectra with published photon-excited spectra,[9-13] most of which are uncorrected even for incoherent-loss structure (background), indicates agreement in the overall shapes of the spectra. The major differences are in the lack of a clear resolution of the C and D peaks in our L_3VV spectrum, and in the presence of an extra (E') peak. The shoulder at the C-peak position became somewhat more distinct with a larger number of deconvolution iterations than the 4-iteration results shown in Figs. 2 and 3, and the D-C separation given in Tables I and II was determined from such higher-iteration curves. With increased number of iterations, however, oscillations—primarily in the region of the E peak—distorted the deconvolution results. These oscillations were indicative of an instrumental resolution comparable in width to the lines to be restored by deconvolution.[20] At 1000 eV the resolution of our analyzer is only 4 eV and thus such resolution limitations for peaks narrower than 4 eV are to be expected. These oscillatory distortions are insignificant for the 4-iteration results given in Figs. 2 and 3, except in causing the sharpness of the E'-peak structure, which could perhaps be an artifact of the deconvolution. No such instabilities were observed in the MVV results discussed below where 10 iterations were always used in deconvolution. Further comparisons of the peak splittings in our $L_{2,3}VV$ spectra with those in published photon-excited spectra[9-13] are given in Table I, with the strongest (D) peak used as the reference for energy separations. Except for the weak A and H peaks, our splittings are in reasonably good agreement with the photon-excited results. No attempt will be made to compare the absolute energy locations of the spectral features because our energy values have not been corrected for the work function of the spectrometer.

Comparisons of our experimental peak separations with term splittings calculated on an atomic model basis, considering direct $L_{2,3}VV$ transitions only, are given in columns (c) and (d) of Table II. Once again the D peak is taken as the reference peak and it is assumed that it is the

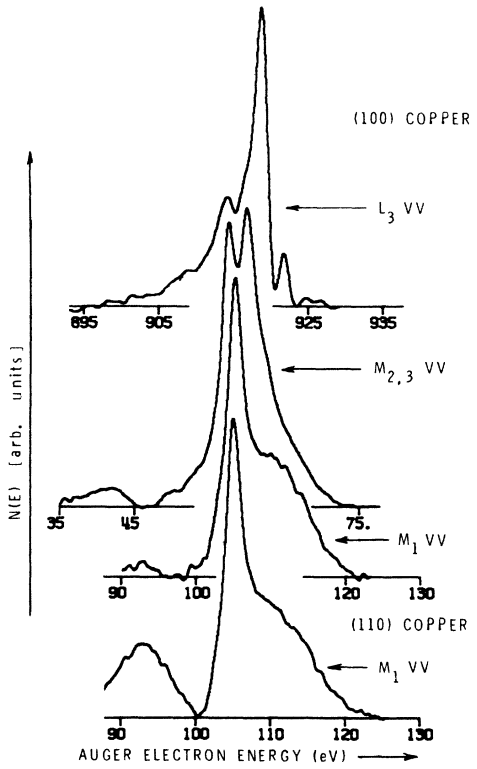

FIG. 3. Deconvoluted L_3VV (4 iterations), $M_{2,3}VV$ and M_1VV (both 10 iterations) spectra from a clean (100) surface. A M_1VV (10 iterations) spectrum from a (110) surface is also plotted for comparison of its low-energy features with those of the (100)-M_1VV signal. The L_3VV spectrum was taken with a 3000-eV primary beam energy while all of the MVV signals in this figure were recorded with a 1500-eV beam energy.

TABLE I. Experimental $L_{2,3}VV$ peak separations (eV).

Peak label	a	b	c	d	e	f
A	−9.8 (?)[g]	NR[h]	−7.5	NR	−7.6	−7.5
B	−4.5	−4.2	−4.5	−4.4	−4.3	−4.1
C	−2.3 (?)	−2.7	−2.25	−2.2	−2.4	−2.6
D	← Reference peak (0.0) →					
E	+3.0	+2.8	+2.6	+2.6	+2.8	+2.8
F	+16.0	+15.5	+16.1	{+14.8, +16.2}[i]	+16.1	+16.2
G	+19.8	+19.5	+19.7	+19.8	+19.7	+19.8
H	+23.1 (?)	NR	NR	+22.6	NR	+22.4

[a] Our measurements.
[b] Yin *et al.* (Ref. 9).
[c] Schön (Ref. 10).
[d] Kowalczyk *et al.* (Ref. 11).
[e] Roberts *et al.* (Ref. 12).
[f] Antonides *et al.* (Ref. 13).
[g] Question mark: poorly defined peak.
[h] NR: not reported.
[i] Double peak.

major peak in the $3d^8$ final-state-configuration calculations for the L_3VV spectrum.[9,11] It is further assumed that the G peak similarly corresponds to the major peak in the direct L_2VV spectrum and that its separation from the D peak should be 19.6 eV, the L_2-L_3 copper core-level splitting from XPS measurements.[23] The experimental G-D peak separation confirms this inter-

TABLE II. Experimental and atomic-model-calculation values of $L_{2,3}VV$ peak separations (eV).

			Calculations without satellite structure		Calculations with satellite structure	
	a	b	c	d	e	f
	Peak label	Experimental splittings	Ion potential	Neutral atom potential	Ion potential	Mixed potential
	A	−9.8 (?)[g]	NP[h]	NP	−6.0 (Satellite)	NP
	B	−4.5	−6.1 ($^1S_0$)	−4.5 ($^1S_0$)	−4.5 (Satellite)	−4.4 (Satellite)
L_3VV	C	−2.3 (?)	−1.2 ($^1G_4$)	NP	−2.8 (Satellite)	{−2.8, −2.0}[i] (Satellites)
	D	← Reference peak →	($^3P+{}^1D_2$)	($^1G_4+{}^3P+{}^1D_2$)	← ($^1G_4+{}^3P+{}^1D_2$) →	
	E	+3.0	+2.1 (^3F)	+3.0 (^3F)	+3.0 (^3F)	+3.0 (^3F)
	F	+16.0	{+13.5($^1S_0$), +18.4($^1G_4$)}[j]	+16.1 ($^1S_0$)	+17.6 (Satellite)	+17.9 (Satellite)
L_2VV	G	+19.8	← from XPS L_2-L_3 splitting = 19.6 → ($^3P+{}^1D_2$)	($^1G_4+{}^3P+{}^1D_2$)	← ($^1G_4+{}^3P+{}^1D_2$) →	
	H	+23.1 (?)	+21.7 (^3F)	+22.6 (^3F)	+22.7 (^3F)	+22.2 (^3F)

[a] Peaks A–E are considered part of the L_3VV spectrum and peaks F–H are considered part of the L_2VV spectrum.
[b] Our measurements.
[c] Yin *et al.* (Ref. 9).
[d] Kowalczyk *et al.* (Ref. 11).
[e] McGuire (Ref. 14).
[f] McGuire (Ref. 14).
[g] Question mark: poorly defined peak.
[h] NP: no peak in calculations.
[i] Double peak.
[j] Choice not clear. (Term assignments for the calculated peaks are given in parentheses.)

pretation. The atomic-model calculations were carried out using electrostatic integrals for Cu^{2+} [column (c)],[9] and for neutral Cu [column (d)].[11] Considering these results for the $3d^8$ final-state-configuration calculations alone (no satellite structure), there is clearly better apparent agreement between the L_3VV experimental splittings and the neutral-atom-potential calculations—at least for the B-D and E-D splittings. The A and C peaks are not explained by either atomic-model calculation. Roberts, Weightman, and Johnson[12] have pointed out, however, that even the apparent B-, D-, and E-peak agreement with theory is illusory. Besides failing to give an explanation of the A and C peaks, the atomic-model calculations[12] indicate that the relative intensity of the experimental B peak is more than an order of magnitude too strong. Roberts *et al.* suggested that the L_3VV spectrum in the A-, B-, and C-peak region may actually be satellite structure resulting from L_3-core-hole decays in the "presence" of a previously created $M_{4,5}$ hole leading to a $3d^7$ final-state configuration. They suggested the Coster-Kronig L_2L_3V process as the process that leads to a L_3 hole with an associated $M_{4,5}$ hole.

Antonides, Janse, and Sawatzky[13] have utilized this interpretation of the A-, B-, C-peak structure in a comparison of the Cu and Zn L_3VV line shapes with the Ga L_3VV line shape (where the L_2L_3V transition is energetically forbidden) to ascertain how much of the Cu and Zn L_3VV intensity is due to satellite structure. Then ascribing this satellite intensity as being due initially to L_2-hole creation, they were able to explain the anomalous L_3VV-to-L_2VV integrated-intensity ratios in Cu and Zn on this basis. For copper their measured value of this ratio was reported as 7.6 to 1, but after correction for the $3d^7$ satellite structure this ratio became 1.6 to 1, closer to the value of 2 to 1 expected on the basis of $L_{2,3}$ level multiplicities. Integrating our $L_{2,3}VV$ spectra in Fig. 2 from 923 to 896 eV for the L_3VV component, and from 959 to 931 eV for the L_2VV component, the L_3VV-to-L_2VV intensity ratio from our data is 5.2. This value is reasonably close to the uncorrected ratio of Antonides *et al.*[13] The limits of integration used by Antonides *et al.* were not specified in their paper. Further, it appears that they used two background subtraction steps in handling their copper data but only explicitly discussed one. Thus, comparison of their uncorrected intensity ratio with our value of 5.2 involves some uncertainties.

McGuire[14] has recently calculated the shape, and intensity with respect to the $3d^8$ principal spectrum, of the $3d^7$ satellite structure taking into consideration not only the $L_2L_3M_{4,5}$ Coster-Kronig transition suggested by Roberts *et al.*[12] (and assumed by Antonides *et al.*[13] to be the sole source of the L_3VV satellite structure) but also the related $L_1L_3M_{4,5}$ and $L_1L_2M_{4,5}$ Coster-Kronig transitions. Further assuming, for "best fit" to the L_3VV spectrum of Antonides *et al.*,[13] a separation of 5.2 eV between the "center" of the satellite structure and the D peak of the principal spectrum, McGuire obtained synthesized $L_{2,3}M_{4,5}M_{4,5}$ spectra[14] with peak splittings given in columns (e) and (f) of Table II. For the spectra reported in column (e) McGuire used the ion potential for calculating transition rates. For the spectra reported in column (f) the neutral atom potential was used to calculate the initial-level populations of the $L_{2,3}M_{4,5}$ configuration due to L_1 and L_2 Coster-Kronig transitions, with the ion potential used for calculating all other matrix elements. For the values in Table II, the XPS L_2-L_3 splitting value[23] of 19.6 eV was used to locate the G peak with respect to the D peak rather than the 20-eV value used by McGuire.[14]

Comparing the results in columns (e) and (f) of Table II with the without-satellite-structure results of columns (c) and (d), and with our experimental results [column (b)], one sees that McGuire's spectra do predict a peak at the C position in reasonably good agreement with the C peak location in our experimental L_3VV spectrum. The McGuire results are in better agreement, *vis-à-vis* the C peak, with the L_3VV spectrum of Antonides *et al.*,[13] but this is to be expected since McGuire arbitrarily adjusted the principal-satellite spectra separation for a best fit to the Antonides *et al.* data. The McGuire spectra that best fit the experimental results [column (f)] do not predict an A peak with any of the experimental-splitting values. The A peak, however, is very weak in all experimental spectra and in some instances (see Table I) is unreported. The same comments apply to the H peak although the H peak is part of the L_2VV principal spectrum analogous to the E peak of the L_3VV spectrum and should have an amplitude larger than observed. A more serious discrepancy between McGuire's spectra and experiment is in the location of the F peak. This lack of agreement points up the failure of either of McGuire's spectra to reproduce well the shape of the L_2VV portion of the $L_{2,3}VV$ data. However, McGuire's calculations were aimed primarily at synthesizing the shape of the L_3VV spectrum. This he has done very well, with the spectra represented by the splittings in column (f) considered by McGuire as giving the better fit to the experimental data. This choice between McGuire's two $L_{2,3}VV$ calculated spectra is further supported by a comparison of the calculated L_3VV-to-L_2VV in-

tegrated-intensity ratios with the experimental ratio of Antonides *et al.*[13] This ratio for the spectra calculated using the neutral atom potential for the initial-level populations [column (f) of Table II)] is 7.33, clearly closer to the experimental value of Antonides *et al.* than is the intensity ratio of 3.28 for the spectra using the ion potential for the entire calculation [column (e) of Table II]. Comparisons of McGuire's calculated ratios with our value of 5.2 do not lead to such a clear cut choice. It should be noted once again, however, that McGuire's calculations include an energy separation between the principal and satellite spectra that was chosen for a best fit to the data of Antonides *et al.* Most of the difference between our experimental ratio and that of Antonides *et al.* certainly lies in the differences in methods of handling the background correction problem and possibly also in the choice of integration limits used to define the L_2VV intensity contribution.

B. *MVV* spectra

The total *MVV* spectra from a (110) surface are also plotted in Fig. 2 and separate M_1VV and $M_{2,3}VV$ spectra from the (100)-surface sample are plotted in Fig. 3. No examples of photon-excited *MVV* spectra could be found in the literature with which our spectra could be compared. The only other published high-resolution electron-excited *MVV* data are the uncorrected $dN(E)/dE$ spectra of Barό, Salmerón, and Rojo.[19b] Comparisons of the peak separations between the two peaks of the $M_{2,3}VV$ spectra (M_2 and M_3) and the sharp peak in the M_1VV spectrum from our deconvoluted $N(E)$ data with the corresponding separations between the major features in the $dN(E)/dE$ data of Barό *et al.* are given in Table III. While our M_2-M_3 separation value only differs from the Barό *et al.* value by 0.5 eV, the M_1-M_3 values differ by more than 1 eV. Comparing our M-peak separations with the corresponding XPS core-level separations[23] in Table III one finds agreement within 0.3 eV. If the peaks in the *MVV* spectra are identifiable with the major (D) peak of the L_3VV spectrum, the L_3-M separations from our Auger spectra are as given in Table III. These separations are all about 3 eV greater than the corresponding XPS core-level separations.[23] This suggested that the peaks in the *MVV* spectra might more plausibly be identified with the C or B peaks of the L_3VV spectrum, i.e., with the satellite structure rather than with the principal L_3VV structure. However, the shapes and energy positions of the *MVV* lines did not change appreciably when measured with a primary electron beam energy of 800 eV (below the L-shell thresholds). The sharp features in the $M_{2,3}VV$ spectra also did not change in shape or in energy location with a primary energy of 119 eV (below the M_1-level ionization energy), indicating that the sharp features in the *MVV* spectra are not due to satellite contributions. These *MVV* spectra for primary energies other than 1500 eV are discussed further below.

Comparison of the M_1VV and $M_{2,3}VV$ spectra in Fig. 3 indicates a similarity in the shapes of the sharp features of the spectra. Proceeding on the supposition[24] that the $M_{2,3}VV$ spectra result from the superposition of two signals, M_2VV and M_3VV, that are identical in shape and differ only in relative amplitude and position in energy, the $M_{2,3}VV$ spectra were decomposed into two such signals. The $M_{2,3}VV$-component curve for the (100) surface at 1500 eV is shown as "M_3VV" in Fig. 4(a). The two parameters in this decomposition that were adjusted for a least-squares best fit of the curve synthesized from the two component curves to the original $M_{2,3}VV$ spectra were the M_3-to-M_2 intensity ratio and the M_2-M_3 energy separation. The best-fit values were 1.3 to 1 and 2.7 eV, respectively. The values of these parameters are reason-

TABLE III. *MVV* relative peak positions (eV).

Auger peak separations	AES data a Deconvoluted integral spectra	AES data b Uncorrected derivative spectra	XPS core level separations c
M_1VV-M_2VV	45.0	45.7	45.2(M_1-M_2)
M_1VV-M_3VV	47.5	48.7	47.4(M_1-M_3)
M_2VV-M_3VV	2.5	3.0	2.2(M_2-M_3)
$L_3VV(D)$-M_1VV	813.3	···	810.4(L_3-M_1)
$L_3VV(D)$-M_2VV	858.3	···	855.6(L_3-M_2)
$L_3VV(D)$-M_3VV	860.8	···	857.6(L_3-M_3)

[a] Our measurements.
[b] Barό *et al.* (Ref. 19b).
[c] Kowalczyk (Ref. 23).

ably close to the fairly wide range of values found by Dobbyn, Williams, Cuthill, and McAlister[25] to lead to an analogous decomposition of the soft x-ray $M_{2,3}$ emission spectra of Cu. A recent XPS value of the M_2-M_3 energy separation is 2.2 eV, again a value that is reasonably close to our best-fit M_2-M_3 separation. Note that the apparent M_2-M_3 peak separation in Fig. 3 (Table III) is only 2.5 eV. The discrepancy in peak separation values is due to the overlap of the M_2 and M_3 signals.

The theoretical M_3-to-M_2 intensity ratio was calculated using McGuire's tabulated M-shell[26] and L-shell[27] Auger and Coster-Kronig transition rates (calculated in j-j coupling). With no satellite intensity contribution to either the M_3VV or M_2VV signals, the ratio should be exactly 2.0, the M_3-M_2 level multiplicity. With $M_1M_{2,3}V$ decay channels "feeding" the $M_{2,3}VV$ signals, the theoretical ratio decreases by less than 0.01%. When the $LM_{2,3}V$ decay channels are also "turned on" the theoretical ratio becomes 2.02. Thus, our experimental ratio at $E_p = 1500$ eV is appreciably less than the expected value. For a primary beam energy of 800 eV, the shape of the (100)-$M_{2,3}VV$ signal and the best-fit decomposition parameters were unchanged. With a primary beam energy of 119 eV, on the (110) surface, the high-energy component of the $M_{2,3}VV$ signal became more extended than in its higher-excitation-energy counterpart, or even in the M_1VV signal—although the best-fit decomposition parameters were essentially unchanged. This $M_{2,3}VV$-component curve for the 119-eV excitation energy is plotted in Fig. 4(b). The broad high-energy feature in this curve is due to characteristic-loss structure, associated with the 119-eV primary-beam electrons, that was not removed by applying the smooth background function used in the Sickafus background subtraction technique.[22] This interpretation is supported by the fact that $M_{2,3}VV$-component curve for a 150-eV (only 1.22 times the M_1 ionization level[23]) excitation energy had high-energy features similar to those of the 800-eV and higher excitation energy curves. The shape of the $M_{2,3}VV$ signal and the M_3-to-M_2 ratio, for excitation energies near the M_1 threshold, need to be further investigated using modulation techniques such as those described by Gerlach, Houston, and Park[28] for separating characteristic-loss features from the AES signals. Such techniques were not used in the measurements reported in this paper.

The fact that the M_3-to-M_2 intensity ratio remained unchanged at 1.3 to 1 with changes in primary beam energy is an indication that satellite-intensity contributions play a negligible role in determining this ratio. This fact is supported by the relative insensitivity of the theoretical ratio to the "turn-on" of $M_1M_{2,3}V$ and $LM_{2,3}V$ satellite decay channels. That the experimental ratio is less than 2 to 1 could very well be an indication that the M_2VV and M_3VV line shapes are significantly different, contrary to the supposition used in the decomposition here and in the work of others.[24] Without satellite-intensity contributions one would expect the M_3VV-to-M_2VV integrated-intensity ratio to be 2 to 1.

With the exception of the 119-eV result, the shapes of the MVV signals from a given surface were unchanged with changes in primary beam energy up to an energy of 3000 eV. The shapes of the MVV signals from the two surfaces were also identical with the one exception that the M_1VV signal from the (110) surface had a broad feature *below* the sharp peak that was not evident in the M_1VV signal from the (100) surface. A M_1VV signal from the (110) surface is plotted in Fig. 3 along with the MVV signals from the (100) surface. The source of this low-energy broad feature is not clear but, as noted above, its presence in the (110)-M_1VV spectrum is not dependent on L-shell vacancies. This broad low-energy feature will not

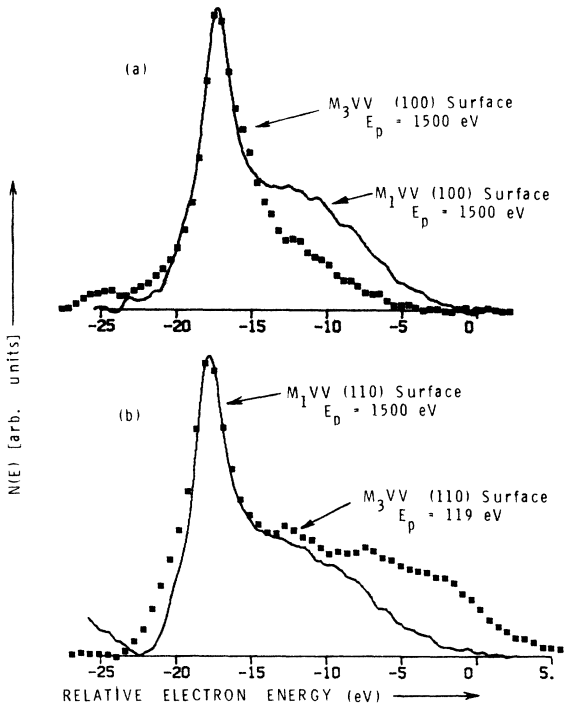

FIG. 4. Comparison of M_1VV (solid curves), and $M_{2,3}VV$-component (dotted curves) spectra. (a) (100) surface results with both spectra recorded at 1500-eV primary beam energy; (b) (110) surface results with the M_1VV spectrum recorded at 1500 eV and the $M_{2,3}VV$ spectra from which this component curve comes recorded at 119 eV.

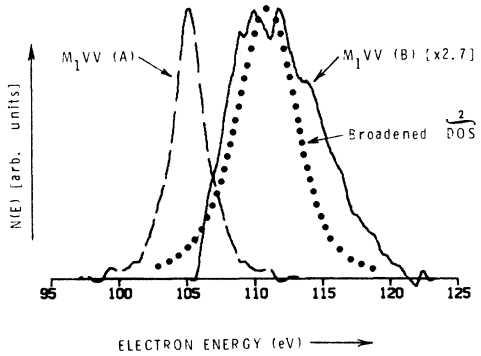

FIG. 5. Decomposition of a (100)-M_1VV spectrum into a symmetric low-energy atomic like peak (dashed curve) and a broad high-energy signal (solid curve). Also plotted (dotted curve) is the self-fold of the copper theoretical DOS (Ref. 29) after being broadened by convolution with a Lorentzian function of 2.09-eV FWHM. The symbol above the theoretical DOS label indicates that the curve plotted in this figure is the self-fold of the theoretical DOS curve.

be considered in the $M_{2,3}$-to-M_1 integrated-intensity calculations presented below.

Also plotted in Fig. 4 along with the "M_3VV" components are the M_1VV signals from the (100) and (110) surfaces taken at 1500 eV. The M_1VV signals are similar to the "M_3VV" curves in the sharp peak regions but differ appreciably in the high-energy region where the M_1VV signal exhibits a distinct broad shoulder for all primary beam energies. This difference suggested a decomposition of the M_1VV spectrum into a sharp *symmetric* low-energy peak and a broad high-energy signal. The results of this decomposition, based on the supposition that the broad high-energy signal does not extend below the peak position of the sharp feature, are shown in Fig. 5. Comparison of the broad signal with the self-fold of the total DOS of copper[29] (Fig. 5) indicates that the broad signal is *too broad* to be a representation of the total copper valence-band DOS. The self-fold of the theoretical total DOS has been convoluted with a Lorentzian function of 2.09-eV full width at half-maximum (FWHM)[21] in Fig. 5 to allow for M_1-lifetime broadening. The width of the experimental broad feature in Fig. 5 is roughly consistent with the width of the self-fold of the s or p valence-band states[30] but the numbers of s and p valence electrons relative to d electrons are meager and an identification of the broad features in the M_1VV signal with s and/or p valence electrons in this way is improbable. An alternative explanation of the shape of the M_1VV signal will be discussed below in our considerations of the recent theoretical calculations of Cini[16] and of Sawatzky.[18]

The $M_{2,3}$-to-M_1 integrated-intensity ratio can be obtained from the MVV spectra in Fig. 2 and compared with theoretical values. Integrating the MVV signals in Fig. 2 from 124.6 to 100.0 eV for the M_1VV intensity, and from 75.0 to 50.0 eV for the $M_{2,3}VV$ intensities, one obtains an integrated-intensity ratio $I(M_{2,3}VV)/I(M_1VV)$ of 17.9 to 1. This integration for the M_1VV signal excludes the broad low-energy structure seen for the (110) surface and not for the (100) surface. That this ratio is much larger than the $M_{2,3}$-M_1 level multiplicity is not surprising, since the principal M_1 decay modes are[21] $M_1M_{2,3}M_{4,5}$ rather than $M_1M_{4,5}M_{4,5}$. These processes would lead to enhanced $3d^7$ final-state-configuration decays for the $M_{2,3}VV$ transition. $L_3M_{2,3}V$ decays are also reported to give an appreciable contribution to the copper Auger spectra.[31]

The MVV spectra in Fig. 2 were recorded with a primary beam energy of 1500 eV. In order to experimentally assess the influence of satellite-intensity and of ionization-cross-section effects in these MVV spectra the spectra were also recorded with primary beam energies of 800 eV (below the L-shell ionization thresholds) and 3000 eV. The integrated-intensity ratios, $I(M_{2,3}VV)/I(M_1VV)$, are given in Table IV. Two measurements at 800 eV give an indication of the reproducibility of the measurements.

The theoretical ratios calculated in j-j coupling are also given in Table IV. Although pure j-j coupling should not be applicable[32] for Cu, a fairly complete[33] tabulation of M-shell[26] and L-shell[27] Auger and Coster-Kronig transition rates, calculated in j-j coupling, exist in published literature and, while the absolute values of the theoretical ratios may be in considerable error,[34] it is expected that the direction of the changes in the ratio with the "turn-on" of the L-shell satellite-decay channels is correctly given. The intensity contributions from the various decay channels have been normalized such that the $I(M_{2,3}VV)$-to-$I(M_1VV)$ ratio without satellite contributions equals 3.0. For each MVV signal, intensity contributions are given by $I_i(\alpha) = N_i A_i(\alpha)/A_i^T$, where α denotes a contribution to either the M_1-, M_2- or M_3-VV signal, i indicates the subshell of the initial core-hole vacancy, and A_i^T is a normalizing factor denoting the total transition rate for all transitions originating from the i-subshell vacancy. N_i are the initial numbers of holes in the ith subshell; initially the relative N_i values were assumed to be simply proportional to the number of electrons in the various subshells, while in a second calculation variations from this level multiplicity distribution due to variation in ionization cross section were estimated using the results of Vrakking and Meyer.[35]

TABLE IV. Comparisons of experimental and theoretical $I(M_{2,3}VV)$-to-$I(M_1VV)$ integrated-intensity ratios.

$I(M_{2,3}VV)$-to-$I(M_1VV)$ integrated-intensity ratios	Primary beam energies 800 eV	800 eV	1500 eV	3000 eV
Experimental ratio	26.3	24.6	17.9	21.6
Satellite channels	$M_1M_{2,3}V$	$M_1M_{2,3}V$	$M_1M_{2,3}V$ and	$LM_{2,3}V$
Theoretical ratio				
Without ionization cross-section terms	43.2	43.2	34.6	34.6
With ionization cross-section terms	54.9	54.9	46.5	42.2
Percent of $M_{2,3}VV$ signal due to satellite intensity				
Experimental percent[a]	22.8	21.9	...	...
Theoretical percent				
Without ionization cross-section terms	23.3	23.3	38.1	38.1
With ionization cross-section terms	18.3	18.3	24.6	31.2

[a]Experimental percentages were based on the assumption that the experimental ratio should be 3 to 1 without satellite-intensity contributions to either the $M_{2,3}VV$ or M_1VV signals. This percent value could only be reliably calculated for the 800-eV signals where the intensity lost from the M_1VV signal appears in the $M_{2,3}VV$ signals.

For the $M_{2,3}VV$ signal the possible intensity contributions come from direct $M_{2,3}VV$ decays as well as from $M_1M_{2,3}V$, and $L_{1,2,3}M_{2,3}V$ satellite decay channels. For the M_1VV signal the intensity contributions include the direct M_1VV decays and the $L_{1,2,3}M_1V$ satellite decays. The theoretical ratios, both with and without the estimated effects of ionization-cross-section variations with energy, show a decrease with the "turn on" of the L-decay-satellite channels. A decrease is also seen in the experimental ratio in going from a primary electron energy of 800 eV to either 1500 or 3000 eV.

The increase in the experimental ratio in going from 1500 to 3000 eV is not seen in the theoretical ratios when the effects of ionization efficiency are included. This is possibly due to the neglect of a potentially important variable in the theoretical calculation—the intensity contributions to the various signals due to the spectrum of electrons backscattered from layers below the surface layer and variations in this backscattered-electron contribution with primary beam energy and with Auger transition energy. No simple method of estimating the influence of these backscattered electrons could be found and this factor can only be explored with a more extensive set of measurements.[36]

In Fig. 6 the M_1VV and "M_3VV" curves from Fig. 4(a) have been replotted together with McGuire's recently[21] calculated atomic-model line shapes for these transitions. In all cases the curves have been normalized to equal peak heights. In contrast to our use above of the pure j-j coupling results, the appropriate transition rates for these curves were calculated in intermediate coupling and the effects of configuration interactions on the line shapes were shown to be negligible.

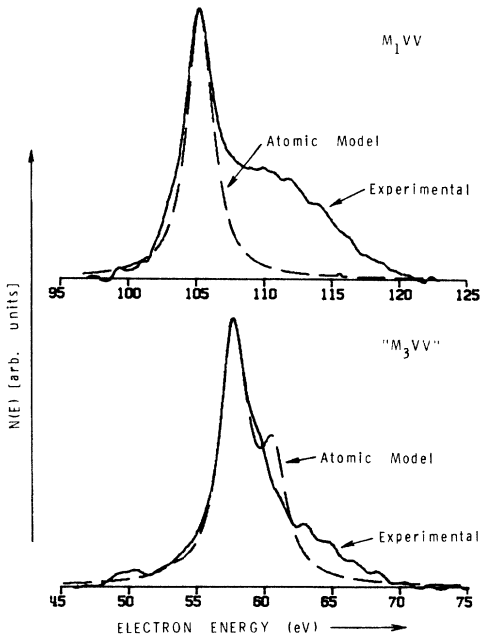

FIG. 6. Comparison of experimental (solid curves) and theoretical (dashed curves) M_1VV- and $M_{2,3}VV$-component spectra for copper. The M_1VV and M_3VV theoretical curves are from atomic-model calculations (Ref. 21) which used matrix elements evaluated at 18 and 40 eV, respectively.

For the theoretical line shapes in Fig. 6, the matrix elements used in the calculation were evaluated at 18 and 40 eV for the M_1VV and $M_{2,3}VV$ spectra, respectively. These energy values are appreciably smaller than those expected on the basis of experimental measurements and a possible source of this discrepancy is discussed in McGuire's paper.[21] Comparison of the experimental and theoretical curves in Fig. 6 reveals very good agreement in the sharp peak regions but considerable disagreement in the higher-energy broad features, particularly for the M_1VV spectra. These differences may indicate that there are remnants of information related to the initial-state $3d$-electron distribution in the experimental MVV signals. A possible valence-band-theory explanation for this juxtaposition of atomiclike and bandlike features is discussed below.

C. Comparisons with other valence-band spectroscopies and with valence-band theory

It is clear from a comparison of the self-fold of the total copper valence-band DOS (Fig. 5) with the $L_{2,3}VV$ and MVV spectra (Fig. 2) that most features in the Auger spectra are too narrow to allow a simple correlation between the unperturbed copper valence band and the shapes of the Auger lines. Feibelman and McGuire[37] have shown that including transition matrix elements to calculate the transition DOS for the $M_{2,3}VV$ and L_3VV copper transitions does not improve the comparison between the band theory and experiment. However, the success of the atomic-model calculations in explaining most aspects of the shapes of the $L_{2,3}VV$ and MVV signals from copper is surprising. The fact that AES is expected to give solid-state valence-band information for metals prompts further comparisons of the shapes of the copper Auger lines with the results of other valence-band spectroscopies and with valence-band theory. These comparisons are further prompted by the conjecture of Barð *et al.*[19b] that the MVV line shapes do contain information on the unperturbed d valence band of copper along with the atomiclike features.

In Fig. 7 examples of valence-band spectra from soft-x-ray emission spectroscopy (SXS), XPS, and ultraviolet photoelectron spectroscopy (UPS) are presented along with our M_1VV and L_3VV spectra. Because the final state configurations for the direct SXS, XPS, and UPS data involve a single hole in the valence band while the AES direct spectra involve two holes, the self convolutions of SXS, XPS, and UPS curves are plotted in Fig. 7 for comparison with our AES results. Also plotted in Fig. 7(d) is the self-fold of the copper total DOS,[29] and in order to emphasize the actual narrowness

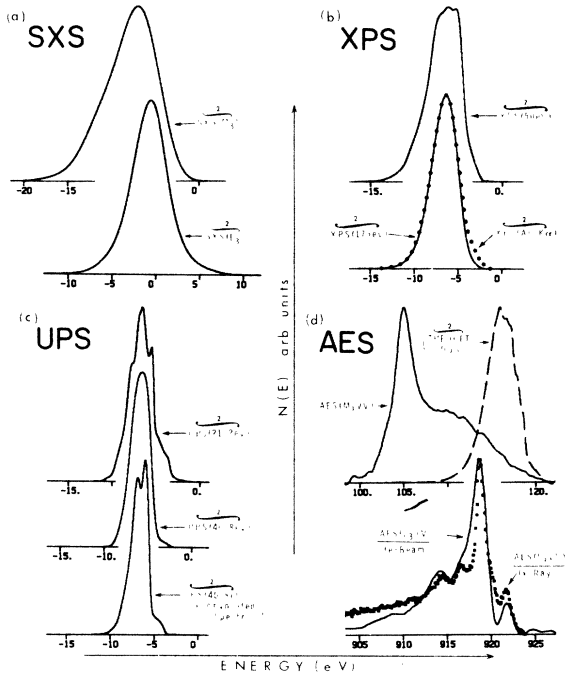

FIG. 7. Comparison of M_1VV and L_3VV AES line shapes (7*d*) with the results of other valence-band-spectroscopic investigations of copper. (a) Self-folds of M_3 (Ref. 25) and L_3 (Ref. 38) soft-x-ray emission spectra. (b) Self-folds of XPS valence-band curves recorded (solid curves) with 50- and 175-eV incident photons (both Ref. 39) and (dotted) with Al $K\alpha$ radiation (Ref. 41). (c) Self-folds of UPS electron distribution spectra recorded (upper two curves) with 21.2- and 40.8-eV photons (both Ref. 42) and the self-fold of a deconvoluted 40.8-eV UPS spectrum (lower curve, Ref. 43). (d) Our M_1VV (upper solid curve) and L_3VV (lower solid curve) AES results plotted together with the self-fold (dashed curve) of the theoretical total DOS (Ref. 29) and an x-ray-excited (dotted curve) L_3VV spectrum (Ref. 12). The symbol above the SXS, XPS, UPS, and theoretical curve labels indicate that the curves plotted in this figure are the self-folds of the original data.

of the D and E peaks in the L_3VV AES spectrum, the x-ray-excited L_3VV spectrum of Roberts *et al.*[12] has been plotted as squares on top of our L_3VV curve. Background corrections of the SXS, XPS, and UPS curves before self-convolution were all as performed by the original workers.

In Fig. 7(a) the self-fold of the M_3-component curve resolved from the $M_{2,3}$ soft-x-ray emission profile for Cu by Dobbyn *et al.*[25] and the self-fold of the L_3-emission curve of Liefeld[38] are given. Both of these curves are broader than the self-fold of the theoretical DOS [Fig. 7(d)] and neither exhibit any sharp structure. Energy-dependent screening and level-broadening effects were suggested by Dobbyn *et al.* as being respon-

sible for the differences between the two experimental curves and between the experimental results and the theoretical DOS. Plotted in Fig. 7(b) are the self-folds of two XPS energy distribution curves recorded by Stöhr, McFeely, Apai, Wehner, and Shirley[39] using synchrotron radiation of energy $h\nu = 50$ and 175 eV. The variations of the experimental curves with photon energy are thought to arise in XPS, and in UPS [Fig. 7(c)], from variations in energy-dependent transition matrix elements and from "final-state effects."[40] Stöhr *et al.* invoked final-state momentum broadening in order to realize better agreement between their XPS experiments [Fig. 7(b)] and theory.[38] For photon energies above 70 eV, the changes in line shape of the XPS curves with changes in energy are less dramatic than the changes that occur at lower energies. This result is illustrated by the comparison in Fig. 7(b) of the 175-eV results with a curve taken with Al $K\alpha$ radiation (1486.6 eV).[41] All of the XPS curves are seen to be comparable in width with the self-fold of the total DOS [Fig. 7(d)] and not to have any sharp structure.

The self-convoluted UPS curves in Fig. 7(c) are narrower than the self-fold of the theoretical total DOS [Fig. 7(d)] and two of the curves have sharp features that are as sharp as some of the features of the AES curves [Fig. 7(d)]. The upper two UPS curves are from data taken recently by Tibbetts, Burkstrand, and Tracy[42] using He I (21.1 eV) and He II (40.8 eV) radiation. The bottom curve in Fig. 7(c) is the self-fold of a deconvoluted He II spectrum reported by McLachlan, Liesegang, Jenkin, and Leckey.[43] Deconvolution was used to remove instrumental broadening and this curve may be seen to have sharp features that are not resolved in the He II spectrum of Tibbetts *et al.* Despite the fact that these UPS curves are narrow in overall width and have sharp features as sharp as those in the AES data, no atomic-model interpretations of these data have been suggested. The sharp features in photoelectron spectra move with changing photon energy indicating that they are the results of conservation of crystal momentum[44] rather than of localized (i.e., atomiclike) structure in the DOS. In 1974 Eastman[40] reviewed UPS measurements for Cu using synchrotron radiation with energies from $h\nu = 8$ to 26 eV and concluded that the experimental spectra were in "quite good" agreement with theoretical spectra derived from the band-structure calculations of Janak, Williams, and Moruzzi.[29]

Thus, the SXS, XPS, and UPS data for Cu are fairly adequately explained by band calculations. The question then arises as to why atomic-model calculations have been more successful than band calculations in explaining the Auger line shapes for Cu. What is different in AES from SXS, XPS, and UPS? The obvious answer to this question lies in the two-hole final-state configuration for the direct Auger spectra. Cini[16] and Sawatzky[18] have recently given independent discussions of the effects of the Coulomb interaction between these two valence-band holes on the shape of an Auger CVV line.

Cini[16] finds that the expected Auger line shape $N^0(E)$ will be distorted to a new form given by

$$N(E) = N^0(E)/\{[1 - WG^0(E)]^2 + \pi^2 W^2 N^0(E)^2\} ,$$

where $G^0(E)$ is the Hilbert transform of $N^0(E)$ $[= \pi^{-1} \int_{-\infty}^{\infty} N^0(E')(E' - E)^{-1} dE']$ and W is the repulsion energy for the two valence-band holes. Assuming that $N^0(E)$ is the self-fold of the Cu total DOS,[29] normalized to unity, a slight difference in shape between $N^0(E)$ and $N(E)$ may be seen for a W as small as 0.3 eV. In Fig. 8, $N(E)$ is plotted for W values of 6.0, 18.2, and 30.0 eV. Also plotted for comparison (dashed curve) is $N^0(E)$, the self-fold of the total DOS.[29] One sees that as W increases $N^0(E)$ becomes more and more distorted in shape and a sharp feature develops at the low-

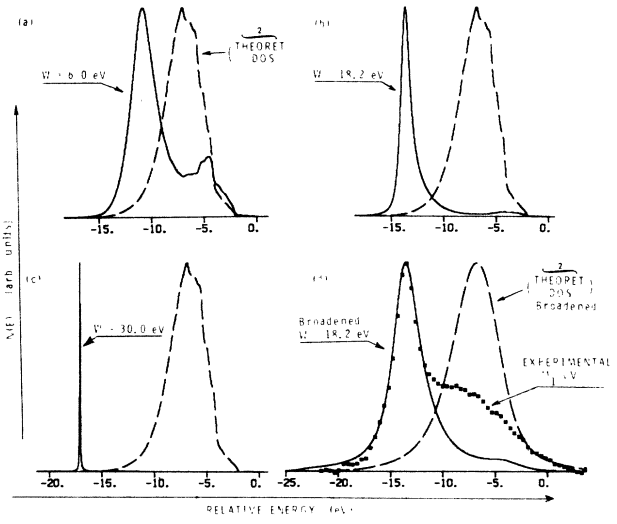

FIG. 8. Distortions (solid curves) to the self-fold (dashed curves) of the total copper DOS (Ref. 29) resulting from electron-correlation effects calculated using Cini's equation (Ref. 16). In (a)–(c) the results for $W = 6.0$, 18.2, and 30.0 eV without core-level-lifetime broadening, are plotted, respectively. In (d) both curves from (b) have been broadened by convolution with a 2.09-eV FWHM Lorentzian function and are compared with our (100) M_1VV signal (dotted curve). The symbol above the theoretical DOS label indicates that the curve plotted in this figure is the self-fold of the theoretical DOS curve. The area under the DOS curve has been normalized to unity.

energy end of the original signal. This sharp feature becomes sharper with increasing W and eventually a localized atomiclike state splits off from the low-energy end of the original signal and the residual intensity in the region of the original signal goes to zero [Fig. 8(c)]. With further increases in W, the localized state moves further and further away from the Fermi-energy location. Since these atomic features will be expected to be broadened due to the finite lifetime of the core-hole state, the $W = 18.2$ eV results from Fig. 8(b) were broadened by convolution with a Lorentzian function of 2.09-eV FWHM[21] for comparison with the experimental (100)-M_1VV signal from Fig. 3. This comparison is shown in Fig. 8(d). It is apparent that the broadened $N(E)$ signal is in good agreement with the experimental curve in the sharp peak region and that $N(E)$ does have a broad high-energy shoulder. This broad feature is not as intense as the experimental broad feature. This discrepancy may be explainable in terms of our complete neglect of the effects of energy- and symmetry-dependent transition matrix elements.

Sawatzky[18] does not provide a simple analytic expression, such as the Cini equation above, for relating $N(E)$ and $N^0(E)$. He does provide guidelines, however, with which the value of W may be estimated from experimental data. He concludes from his calculations that the integrated-intensity ratio R of the sharp feature in the distorted signal to the broad feature will be given approximately by $(W/B)^2 - 1$, where B is the width of the undistorted valence band and W is once again the hole-hole interaction energy. The width of the sharp peak in the distorted signal b, will be of the order of B^2/W. With these two estimates one finds that the hole-hole repulsion energy should be given approximately by $W = b(R + 1)$. Using the results from our decomposed M_1VV signal (Fig. 5: $R = 1.1$ and b is the FWHM of the sharp feature, = 2.62 eV) one finds that W has a value of 5.5 eV. This value is smaller than the best-fit value, 18.2 eV, obtained using Cini's equation and the same experimental M_1VV data. 5.5 eV is also somewhat smaller than the value of $W = 8.0$ eV determined by Sawatzky and Antonides[15] from conservation-of-energy considerations relating the energy of their $L_3VV(D)$ peak[13] to energy values for the $2p$ and $3d$ XPS lines of copper.

IV. SUMMARY AND CONCLUSIONS

Our electron-excited $L_{2,3}VV$ spectra are in good agreement with x-ray-excited examples of these spectra.[9-13] Two mechanisms that account for the shape of the L_3VV signal[14] are now generally accepted. The multiplet splitting mechanism explains the separation and relative intensities of the two high-energy peaks D and E. The shape of the lower energy portion of the signal is ascribed to the occurrence of Coster-Kronig L_1L_3V and L_2L_3V transitions preceding the decay of the L_3 hole. This means that some of the L_3 holes decay in the presence of "spectator" $3d$ holes which leads to a $3d^7$ final-state configuration. Splittings and intensity ratios for this configuration have been calculated by McGuire[14] and used to synthesize the total, direct plus satellite, L_3VV spectrum. The satellite intensity in the L_3VV spectra has also been used to explain the anomalous L_3-to-L_2 integrated-intensity ratios of Antonides *et al.*[13] and our experimental results are in reasonable agreement with theirs.

The atomic-model calculations of McGuire are less successful is reproducing the line shape of the L_2VV spectrum. Antonides *et al.* used a background correction scheme[45] that does not allow for structure in the characteristic-loss signal. This could be a source of some of the discrepancy between their L_2VV spectrum and McGuire's synthesized curves. Our MVV line shapes are also poorly reproduced by McGuire's calculations[21] except in the region of the sharp peaks. Thus the discrepancies between McGuire's MVV calculated line shapes and our spectra lie mainly in the broad high-energy features seen in the experimental data and not in the calculated curves. These broad features suggest a valence-band explanation. They are not simply related to the unperturbed d-band DOS as has been suggested by Barδ *et al.*[19b] They are too broad for such an explanation.

Integrated-intensity ratio calculations for the MVV spectra indicate that satellite intensity does contribute to the $M_{2,3}VV$ and M_1VV lines. Measurements at differing electron-beam excitation energies, however, indicate that this satellite intensity does not result in additional structure (peaks) in the MVV spectra as it does in the L_3VV signal. Thus, the sharp features in the MVV spectra are explained by direct-transition atomic-model arguments while the broad feature presents an anomaly.

The electron-correlation-effect arguments of Cini[16] and of Sawatzky[18] offer an appealing explanation to this anomaly. Not only do they give a qualitative explanation of the presence of atomiclike *and* bandlike features in the MVV line shapes that is very good, but they offer a physical explanation of the fact that the CVV lines from some metals are bandlike while the lines from other metals are atomiclike. The best-fit comparison of our M_1VV spectrum with a Cini distorted curve resulted in a hole-hole repulsion-energy estimate of 18.2 eV. This value is more than twice the estimate of 8 eV obtained by Sawatzky and Antonides[15] from L_3VV

data, and more than three times the estimate, 5.5 eV, that we get from analyzing our M_1VV data in terms of Sawatzky's arguments.[18] In comparing the Cini model with our experimental MVV results, the assumption was made that the hole-hole repulsion does not significantly mix angular momentum, and hence that the area under the theoretical DOS curve should be equal to unity. (The DOS curve is thus regarded as some average DOS function for Cu.) The value of W that is obtained by fitting the theoretical curve to the data depends inversely on the area under the $N^0(E)$ function and, for a CVV signal, inversely on the square of the area under the DOS function. The opposite, and on first consideration perhaps plausible, assumption that the valence bands of Cu are completely degenerate, and that the area under $N^0(E)$ should be equal to the square of one half the number of copper valence electrons per atom, leads to an unphysical W estimate of 0.6 eV. If significant line shape distortion of the type discussed by Cini and by Sawatzky could occur for hole-hole repulsion energies less than 1 eV one would expect that the CVV lines for all metals would be atomiclike.

The discrepancy between the W estimates from comparisons with Cini and with Sawatzky needs further investigation. In comparing the Cini model with the Cu experimental data one must determine what modifications must be made to account for the fact that Cu has some ten d-band electrons rather than a single simple two-electron band as considered in the paper by Cini. The 5.5-eV W estimate from comparison with Sawatzky may also be in some error since the Sawatzky equations used to get that value were based on an expansion that assumed W to be much greater than twice the valence-band width. The influence of transition matrix elements and of dynamic screening on the Cini-Sawatzky arguments may also be important. The detailed effects of screening in a metal will depend on the velocity of the Auger electron and hence the strength of the hole-hole repulsion-energy effects may vary from AES transition to transition in a given material. The effects of the surface sensitivity of AES on the results is a subject that must also be considered.

The Cini-Sawatzky arguments offer a promising way of studying electron-correlation effects in metals—especially d-band metals. More detailed comparisons of Auger line shapes with calculated transition DOS, and with predicted effects that the electron correlations may have on the line shapes, are needed. Such comparisons will help sort out the ideas concerning the contributions of band structure versus atomiclike behavior to the Auger line shapes. It is hoped that the results presented in this paper will help stimulate interest in further investigations. Not until one has good agreement between experiment and theory, as apparently exists for the L_3VV copper line shape,[14] should the Auger spectra from a given material be considered understood.

ACKNOWLEDGMENTS

The authors would like to thank the many persons with whom these data were discussed in attempts to understand the copper Auger line shapes. The contributions of E. J. McGuire and of P. J. Feibelman were especially valuable in this regard. The authors are also grateful to the other authors[13, 14, 16–18, 21, 42] who were willing to provide copies of their papers before publication as well as unpublished results. One of the authors (H.H.M.) would like to acknowledge the assistance of J. E. Houston and D. G. Schreiner in the data-reduction procedures. Finally the authors wish also to thank J. F. Cooke of Oak Ridge National Laboratory and A. C. Switendick of Sandia for supplying independent and unpublished calculations of the projected DOS that were very useful in the search (albeit unsuccessful) for direct valence-band-DOS information in the Auger line shapes. This work was supported by the U.S. Department of Energy under Contract AT(29-1) 789. The Oak Ridge National Laboratory is operated by Union Carbide Corporation under contract with the U.S. Department of Energy.

[1]J. J. Lander, Phys. Rev. 91, 1382 (1953).
[2]C. J. Powell, Phys. Rev. Lett. 30, 1179 (1973).
[3]J. E. Houston, J. Vac. Sci. Technol. 12, 255 (1975).
[4]J. E. Houston, G. Moore, and M. G. Lagally, Solid State Commun. 21, 879 (1977).
[5]H. H. Madden and J. E. Houston, Solid State Commun. 21, 1081 (1977).
[6]M. L. Knotek and J. E. Houston, Phys. Rev. B 15, 4580 (1977).
[7]J. M. Burkstrand and G. G. Tibbetts, Phys. Rev. B 15, 5481 (1977).
[8]P. J. Feibelman, E.J. McGuire, and K. C. Pandey, Phys. Rev. B 15, 2202 (1977).
[9]L. Yin, T. Tsang, I. Adler, and E. Yellin, J. Appl. Phys. 43, 3464 (1972); L. I. Yin, I. Adler, T. Tsang, M. H. Chen, D. A. Ringers, and B. Crasemann, Phys. Rev. A 9, 1070 (1974).
[10]G. Schön, J. Electron Spectrosc. Relat. Phenom. 1, 377 (1972, 1973).
[11]S. P. Kowalczyk, R. A. Pollak, F. R. McFeely, L. Levy, and D. A. Shirley, Phys. Rev. B 8, 2387 (1973).
[12]E. D. Roberts, P. Weightman, and C. E. Johnson, J. Phys. C 8, L301 (1975).

[13]E. Antonides, E. C. Janse, and G. A. Sawatzky, Phys. Rev. B 15, 1669 (1977); 15, 4596 (1977).
[14]E. J. McGuire, Phys. Rev. A 17, 182 (1978).
[15]G. A. Sawatzky and E. Antonides, J. Phys. (Paris) Suppl. 37, C4-117 (1976).
[16]M. Cini, Solid State Commun. 24, 681 (1977); 20, 605 (1976).
[17]L. I. Yin, T. Tsang, and I. Adler, Phys. Rev. B 15, 2974 (1977).
[18]G. A. Sawatzky, Phys. Rev. Lett. 39, 504 (1977).
[19](a) M. Salmerón, Surf. Sci. 41, 584 (1974); (b) A. M. Baró, M. Salmerón, and J. M. Rojo, J. Phys. F 5, 826 (1975).
[20]H. H. Madden and J. E. Houston, J. Appl. Phys. 47, 3071 (1976); Adv. X-Ray Anal. 19, 657 (1976).
[21]E. J. McGuire, Phys. Rev. A 16, 2365 (1977).
[22]E. N. Sickafus, Rev. Sci. Instrum. 42, 933 (1971).
[23]S. P. Kowalczyk, Ph.D. thesis (University of California, 1976) (unpublished) (Lawrence Berkeley Laboratory Report No. LBL-4319).
[24]This same assumption was used in the atomic-model calculations of McGuire (Ref. 21) and also by Feibelman and McGuire (Ref. 36) in their calculation of the transition DOS for copper.
[25]R. C. Dobbyn, M. L. Williams, J. R. Cuthill, and A. J. McAlister, Phys. Rev. B 2, 1563 (1970).
[26]E. J. McGuire, Sandia Research Report No. SC-RR-710835 (unpublished); Phys. Rev. A 5, 1052 (1972).
[27]E.J. McGuire, Sandia Research Report No. SC-RR-710075 (unpublished); Phys. Rev. A 3, 1801 (1971).
[28]R. L. Gerlach, J. E. Houston, and R. L. Park, Appl. Phys. Lett. 16, 179 (1970).
[29]J. F. Janak, A. R. Williams, and V. L. Moruzzi, Phys. Rev. B 11, 1522 (1975).
[30]J. F. Cooke, Oak Ridge National Laboratory (unpublished).
[31]C. J. Powell and A. Mandl, Phys. Rev. Lett. 29, 1153 (1972).
[32]W. N. Asaad and W. Mehlhorn, Z. Phys. 217, 304 (1968).
[33]No values for the L_2L_3M nor for the LLN_1 Coster-Kronig transition rates are given in McGuire's tables (Ref. 27) and they have been assumed to be negligible in the normalization used in our calculations. A linear interpolation was used to obtain the L-shell rates for Cu from the tabulated rates for Fe and Zn (Ref. 27).
[34]The theoretical $M_{2,3}VV$-to-M_1VV ratios with only the $M_1M_{2,3}V$-satellite-decay channels open, calculated in intermediate coupling and with configuration interaction effects accounted for (using Table 6 of Ref. 21), are 38.7 and 20.4 for use of the neutral-atom potential at 30 and 18 eV, respectively. These values are clearly closer to our experimental 800-eV values than is the theoretical (j-j coupling) value of 43.2 tabulated in Table IV.
[35]J. J. Vrakking and F. Meyer, Phys. Rev. A 9, 1932 (1974).
[36]T. E. Gallon, J. Phys. D 5, 822 (1972).
[37]P. J. Feibelman and E. J. McGuire, Phys. Rev. B 15, 3575 (1977).
[38]R. J. Liefeld, in *Soft X-Ray Band Spectra*, edited by D. J. Fabian (Academic, New York, 1968), p. 133.
[39]J. Stöhr, F. R. McFeely, G. Apai, P. S. Wehner, and D. A. Shirley, Phys. Rev. B 14, 4431 (1976).
[40]D. E. Eastman, in *Vacuum Ultraviolet Radiation Physics*, edited by E. Koch, R. Haensel, and C. Kunz (Pergamon, Vieweg, 1974), p. 417.
[41]C. S. Fadley and D. A. Shirley, in *Electronic Density of States*, Natl. Bur. Stds. Spec. Publ. No. 323 (U.S. GPO, Washington, D.C., 1971), p. 163.
[42]G. G. Tibbetts, J. M. Burkstrand, and J. C. Tracy, Phys. Rev. B 15, 3652 (1977); these authors note (private communications) that the details of the background corrections (unpublished) to their data are important for peak-shape determinations but relatively unimportant for determining peak positions.
[43]A. D. McLachlan, J. Liesegang, J. G. Jenkin, and R. C. G. Leckey, Jpn. J. Appl. Phys. Suppl. 2, 2, 767 (1974).
[44]P. J. Feibelman and D. E. Eastman, Phys. Rev. B 10, 4932 (1974).
[45]A. D. Martin, J. Phys. D 8, 2074 (1975).